Solid State Communications 179 (2014) 1–5

Contents lists available at ScienceDirect

Solid State Communications

journal homepage: www.elsevier.com/locate/ssc

Magnetic order, spin dynamics and transport properties of the pyrochlore iridate $Y_2Ir_2O_7$

Hui Liu, Wei Tong, Langsheng Ling, Shile Zhang, Ranran Zhang, Lei Zhang, Li Pi, Changjin Zhang *, Yuheng Zhang

High Magnetic Field Laboratory, Chinese Academy of Sciences and University of Science and Technology of China, Hefei 230031, China

ARTICLE INFO

Article history:
Received 23 September 2013
Accepted 2 November 2013
by A.H. MacDonald
Available online 9 November 2013

Keywords:
A. Pyrochlore
D. Geometrical frustration
D. Spin–orbit coupling
D. Variable-range hopping

ABSTRACT

In the present paper, we report the bulk magnetization, electron-spin-resonance spectra and transport properties of $Y_2Ir_2O_7$. It is found that $Y_2Ir_2O_7$ exhibits a magnetic transition at $T_c=150$ K and coexistence of antiferromagnetic and ferromagnetic component due to geometrical frustration. The antiferromagnetic order is due to Ir–O–Ir superexchange interactions and the ferromagnetic component is caused by canting of the moments from the antiferromagnetic state. The behavior of spin dynamics confirms that antiferromagnetic ordering with all-in/all-out structure is responsible for the existence of ferromagnetic component. The resistivity reveals that this compound is a semiconductor and the variable-range hopping process dominates the transport mechanism.

1. Introduction

The Iridium–pyrochlore family of compounds, $A_2Ir_2O_7$, spans a broad spectrum of electrical and magnetic properties that make them prime candidates for exploring complex phenomena in solid state chemistry and physics [1]. Such iridates have recently proved to be a fertile ground for studies of new physics driven by the competition between spin and orbit coupling (SOC) and the electron–electron Coulomb interaction U [2]. Since these transition-metal oxides with 5d electrons are characterized by the strong SOC due to the large atomic number of 5d Ir element, the SOC competes with the kinetic and interaction energies, leading to substantial correlation effects despite the relatively extended nature of the 5d orbitals [3].

$Y_2Ir_2O_7$ is a typical pyrochlore iridate, with a structure composed of Ir ions distributed on a network of corner-sharing tetrahedra. The basic characteristic of the electronic structure is that each of four Ir atoms is octahedrally coordinated by six O atoms. This makes the Ir 5d state split into doubly degenerate e_g and triply degenerate t_{2g} states. Due to the extended nature of Ir 5d orbital, the crystal field (CF) splitting between t_{2g} and e_g is large with the e_g band to be 2 eV higher than the Fermi level [4,5]. SOC has a considerable effect on t_{2g} states: it lifts their degeneracy and produces quadruplet with $J_{eff}=3/2$ and doublet with $J_{eff}=1/2$ with the latter lying higher in energy [4–7]. Previous reports showed that $Y_2Ir_2O_7$ is a Mott insulator with a weak ferromagnetic component below 170 K, as a consequence of either a spin-glass ordering or spin canting [8–11]. However, the bulk spectrum of high-resolution photoemission exhibited a substantial intensity at ε_F suggesting metallic phase, which is in sharp contrast to the prediction of the Mott insulating phase [12]. It was recently reported that $Y_2Ir_2O_7$, a candidate of topological insulator, shows no sign of magnetic ordering [13]. However, long-range magnetic order has been found in $Y_2Ir_2O_7$, similar to those observed in $Eu_2Ir_2O_7$ [14] and $Nd_2Ir_2O_7$ [15], as evidenced by the onset of spontaneous muon spin precession below $T_{LRO}=150$ K [16]. Therefore, the nature of the magnetic transition and transport mechanism is not clear at present.

In order to get a deep insight on the magnetic, transport and spin dynamical properties of $Y_2Ir_2O_7$, we carried out detailed studies on this compound using the measurements of the bulk magnetization, electron-spin-resonance spectra and electrical resistivity. It is found that $Y_2Ir_2O_7$ is a unique frustration system that indeed exhibits coexistence of ferromagnetic and antiferromagnetic component. This compound is a semiconductor and the variable-range hopping process is found to best describe the transport behavior.

2. Experiment

Polycrystalline sample $Y_2Ir_2O_7$ was synthesized by solid state reaction route similar to previously reported preparation conditions [17]. High-purity (> 99.9%) stoichiometric amounts of Y_2O_3 and IrO_2 powders were ground together and palletized. The pellet was heated between 1000 °C and 1050 °C for three days in a vacuum silica tube with two intermediate grindings. After

* Corresponding author. Tel.: +86 551 655 95655.
E-mail address: zhangcj@hmfl.ac.cn (C. Zhang).

0038-1098/$ - see front matter © 2013 Elsevier Ltd. All rights reserved.
http://dx.doi.org/10.1016/j.ssc.2013.11.004

adding 10% of IrO_2 in the appropriate molar ratio, the pellet in a vacuum silica tube was heated at 1150 °C for three days with several intermediate grindings. The obtained sample was characterized by powder X-ray diffraction (XRD) with Cu $K\alpha$ radiation at room temperature. The actual composition of the sample was determined using energy dispersive X-ray spectrometry (EDX). The electrical resistivity was measured by a conventional four-probe method. The magnetization was measured using the Quantum Design SQUID magnetometer. The electron-spin-resonance (ESR) spectra were collected with a Bruker EMX plus model spectrometer at 9.40 GHz.

3. Results and discussion

3.1. Structure

Fig. 1 gives the powder XRD pattern of the $Y_2Ir_2O_7$ sample. Rietveld refinement reveals a single cubic phase (a=10.1706 Å; space group *Fd*-3*m*). Energy dispersive X-ray analysis using scanning electron microscopy reveals Y:Ir ratio to be uniform 1:1 throughout the specimen.

3.2. Magnetism

Fig. 2(a) shows the temperature dependence of the magnetic susceptibilities $\chi=M/H$ of $Y_2Ir_2O_7$ for several different applied fields. A divergence can be seen between the zero-field-cooling (ZFC) and field-cooling (FC) magnetization at $T_c=150$ K. The magnetic properties should be attributable to the behavior of the Ir ions in the compound, because the Y ions are diamagnetic. The difference in χ_{FC} and χ_{ZFC} is attributed to the emergence of very weak ferromagnetic (FM) components. However, χ measured under the ZFC condition shows a small sharp peak at T_c, indicating an antiferromagnetic (AFM) ordering, similar to that observed for other members of the *A*-227 family at comparable temperatures [17–19]. It is suggested that a complex magnetic ordering induced by geometrical frustration in the pyrochlore lattice occurs below T_c. For $Y_2Ir_2O_7$, previous reports have suggested that the ferromagnetic component is caused by the spin-glass-like ordering of Ir ions and it is supposed that this spin-glass behavior is due to a geometrical peculiarity of the pyrochlore structure [8–10]. However, this possibility is clearly excluded by the μSR measurements which indicate long-range ordering below 150 K [16]. Normally for conventional spin glasses, the ZFC curve is expected to show

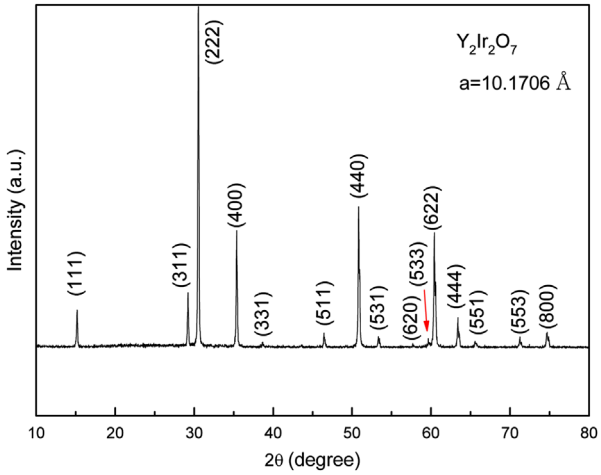

Fig. 1. (Color online) Powder X-ray-diffraction pattern for the $Y_2Ir_2O_7$ sample.

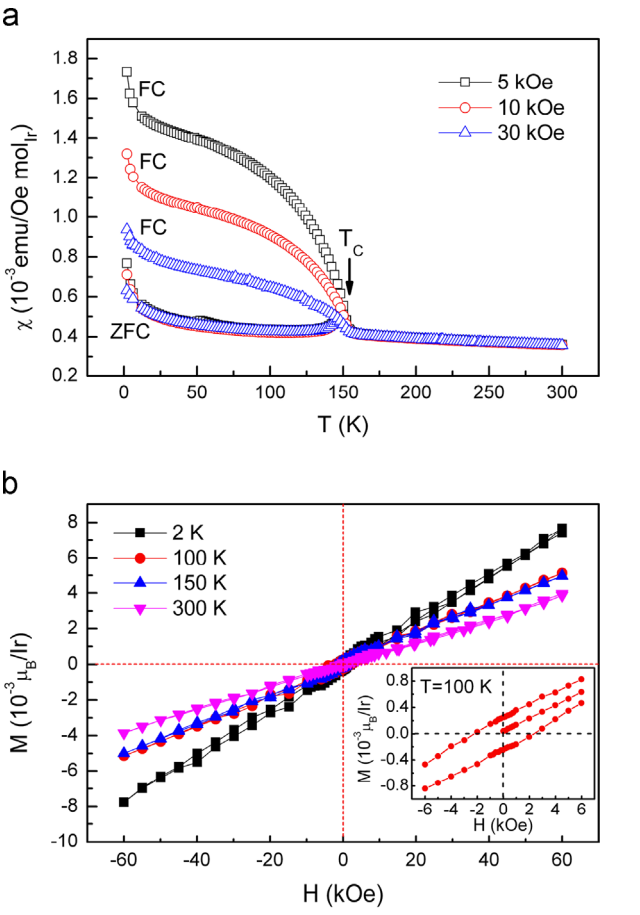

Fig. 2. (Color online) (a) Temperature dependence of the ZFC and FC susceptibility of $Y_2Ir_2O_7$ for applied magnetic fields of 5, 10, and 30 kOe. The magnetic transition at $T_c=150$ K is indicated and (b) magnetization as a function of the applied field at 2, 100, 150 and 300 K. The inset is the expanded view of the low-field portion of the data at $T=100$ K.

a steep decrease below T_c because most spins get frozen at T_c; a sufficiently strong applied field quenches the glass state, and the freezing temperature decreases monotonically and rapidly with increasing applied magnetic field [20]. As can be seen from Fig. 2 (a), the observed behavior of χ_{ZFC} suggests that only a partial fraction of spins freeze if they could freeze. Besides, the temperature of divergence in $Y_2Ir_2O_7$ is only weakly dependent on applied field. In this sense, the transition is not a spin-glass-like transition. It should be noted that the temperature of magnetic transition is different from the previous reports in Refs. [13] and [16], probably because the preparation process is different. The slight upturn in the χ below 25 K may be caused by a small amount of magnetic impurity [8].

The susceptibility above 160 K is well produced using the Curie–Weiss law

$$\chi=\frac{C}{T-\theta_{cw}}+\chi_0 \quad (1)$$

Where C, θ_{cw} and χ_0 are the Curie constant, the Weiss temperature and a constant term independent of temperature, respectively. The best-fitted values are $C=3.69\times10^{-2}$ emu K/Oe mol Ir, $\theta_{cw}=-90$ K and $\chi_0=2.70\times10^{-4}$ emu/Oe mol Ir. The corresponding effective moment $\mu_{eff}=0.54\mu_B$/Ir, significantly lower than Hund's-rule value $1.73\mu_B$ for $S=1/2$. The small Ir moment is also found for the Ir^{4+} cation in the 5M $BaIrO_3$ ($0.215\mu_B$/Ir) [21]. Recent theoretical research has indicated that the consideration of SOC helps to reduce the magnetic moment, thereby, brings the calculated

magnetic moment closer to the experimentally observed value [5]. Therefore, we believe that this reduction of $\mu_{\rm eff}$ originates from the strong SOC of Ir cations. $\theta_{\rm cw}$ is a negative value, suggesting an AFM spin coupling. This is consistent with all-in/all-out (all moments point to or away from the centers of the tetrahedron) magnetic order in the theoretical calculations [4,22]. That is to say, the AFM transition at 150 K is obtained by AFM ordered state with all-in/all-out structure. In fact, μSR research has found that the spins in related compounds $Eu_2Ir_2O_7$ [14], $Nd_2Ir_2O_7$ [15] and $Y_2Ir_2O_7$ [16], form a regularly long-range ordered state rather than a spin-glass, consistent with our results. Due to the extended nature of 5d orbitals, the hybridization of 5d orbitals of Ir and 2p orbitals of O is strong and important for the interatomic exchange interaction. In $Y_2Ir_2O_7$, the Ir–O–Ir bond angle is 129.7° [22], much larger than 90°, so Ir–O–Ir AFM superexchange interaction is dominant, resulting in AFM spin coupling.

The M–H curves measured at 2, 100, 150 and 300 K are displayed in Fig. 2(b). All the curves display paramagnetic (PM) properties of the compound. We also find that a narrow hysteresis loop is observed at $T<T_c$, indictive of a weak FM order (see the inset of Fig. 2(b)). However, at $T=300$ K the curve merely presents a PM component. This is in agreement with the results of χ–T curves. The weak FM order at $T<T_c$ is probably due to canting of the moments from the AFM all-in/all-out state. From the bulk magnetization, we can obtain that the FM component coexists with AFM order in $Y_2Ir_2O_7$ compound. This behavior is caused by a geometrical frustration of the pyrochlore structure.

In order to further investigate the micromagnetism of $Y_2Ir_2O_7$, we measured the ESR spectra because ESR is a sensitive tool to study spin fluctuations and magnetic interactions. In the present measurement, microwave radiation with fixed frequency enters the sample cavity and the external field is swept from 0 to 8000 Oe. In the simplest case, ESR will occur when

$$h\nu = g\mu_B H \tag{2}$$

where h is the Planck constant, g is the electron Landé g factor, μ_B is the Bohr magneton, and H is the applied magnetic field. The g factor for the unpaired electrons is $g_e=2.0023$. According to Eq. (2), the resonance field $H_{\rm res}$ should be located at 3330 Oe for unpaired electrons if there is no internal interaction. The effective magnetic field $H_{\rm eff}$ experienced by the unpaired electrons can be expressed in a simple form as

$$H_{\rm eff} = H_{\rm ext} + H_{\rm int} \tag{3}$$

Here $H_{\rm ext}$ is the applied magnetic field, and $H_{\rm int}$ is the local internal magnetic field. Under the condition of $H_{\rm int}>0$, $H_{\rm int}$ may cause the resonance line to shift to lower field; on the contrary, the $H_{\rm res}$ would appear at higher field with negative internal magnetic field.

The ESR spectra are revealed in Fig. 3(a). There are two resonance signals in the spectra. At temperatures below T_c, the high-field peak, which is marked by a blue arrow at 3352 Oe, is very close to 3330 Oe for a free electron. The location of the peak does not shift with decreasing temperature, thus the PM peak is attributable to Ir spins at grain boundaries. Furthermore, the very weak hyperfine splitting of the spectrum was suggested to be caused by the nuclear spin moments [23]. For the low-field peak (marked by red arrow), the temperature dependence of $H_{\rm res}$ is shown in Fig. 3(b). In the $Y_2Ir_2O_7$ sample, Ir^{4+} is magnetic ion which has $e_g^0t_{2g}^5$ spin configuration [13]. In this configuration, there is one unpaired electrons that can contribute to this ESR absorption. With decreasing temperature from 300 K, the resonance field $H_{\rm res}$ exhibits a slight shift to a lower field. An obvious reduction occurs below 150 K, which indicates that there is a rapid shift of the resonance field toward low field. It suggests that the sample undergoes a weak PM–FM phase transition around 150 K, which is in agreement with the χ–T data. In fact, the weak FM order is due to canting of the moments from the AFM all-in/all-out state and coexists with the AFM ordering. However no ESR signal can be detected if the electrons are under the environment of AFM interaction because the AFM-resonance frequency is far from the X-band. In Fig. 3(c), one can see that the temperature dependence of relative intensity [I(T)/I(300 K)] of the low-field peak decreases upon cooling, signaling the decrease of PM phase. It should be noted that the signal intensity drastically depresses below 150 K, which indicates that below this temperature, the number of unpaired spins contributing to the ESR decreases. It means that a certain number of paramagnetic ions are involved in some kind of magnetic interaction below 150 K. The rapid decrease of resonance intensity at 150 K is related to the emergence of the FM component. However, the FM component coexists with AFM order. Thus, the depression of resonance intensity is possibly due to the enhancement of AFM magnetic fluctuation, as observed in iron-based superconductors [24,25]. The evolution of $H_{\rm res}$ and relative intensity [$I(T)$/I(300 K)] of the low-field peak confirms that the detected ESR signal originates from the $Y_2Ir_2O_7$ sample, but not from some unreacted Ir impurity. The ESR peak-to-peak width ($\Delta H_{\rm pp}$) provides further information on the evolution of the AFM spin fluctuations. A noticeable feature is that the $\Delta H_{\rm pp}$ broadens at low temperature, as shown in Fig. 3(d). The $\Delta H_{\rm pp}$ is determined by the spin-lattice relaxation time T_1 [24]. The $\Delta H_{\rm pp}$ increases rapidly with decreasing temperature below 150 K indicating a shortening of T_1, which is consistent with the strong enhancement of magnetic fluctuation. It is suggested that the enhancement of AFM fluctuations exists below T_c, which is consistent with the μSR results [16]. The ESR measurement confirms that AFM ordering with all-in/all-out structure is responsible for the existence of FM component. It should be noticed that there is an anomaly at low temperatures below 25 K, as displayed in Fig. 3(b)–(d), which may be caused by magnetic impurities.

3.3. Transport properties

Fig. 4 plots the temperature dependence of resistivity of $Y_2Ir_2O_7$. The resistivity exhibits a semiconductor behavior in all the temperature range measured, with a value of approximately 0.03 Ω cm at room temperature, and which exceed 10^5 Ω cm by 10 K. The resistivity neither follows a thermally activated exponential behavior $\rho=\rho_0\exp(E/k_BT)$ as expected for simple semiconductors such as $Y_2Ru_2O_7$ [26], nor does it follow the nearest-neighbor hopping of small polarons, $\rho=\rho_0 T\exp(E_p/k_BT)$. This indicates that no gap is formed at the Fermi level, and carriers are not be coupled by short-range magnetic correlation within a magnetic cluster. We find that the low-temperature ($<T_c$) and high temperature ($>T_c$) resistivity can be fitted by Mott's law of variable-range hopping (VRH) model,

$$\rho=\rho_0\exp(T_0/T)^{1/4} \tag{4}$$

as shown in the inset of Fig. 4. This means that VRH process dominates the transport mechanism at the range of the whole temperature. The VRH process has been observed in resistivities of $Eu_2Ir_2O_7$ [18] and $Nd_2Ir_2O_7$ [27]. The VRH process may be due to two reasons: one is that the local structural disorder and/or the chemical disorder in the polycrystalline sample divides the system into a number of magnetic clusters and induces some fluctuations in both the Coulomb and magnetic potentials, which increases the magnetic scattering and favors the carrier localization; the other is that magnetic fluctuation plays an important role, i.e., the AFM fluctuation will increase the disorder in the magnetic structure of the Ir moments. The μSR measurement of $Y_2Ir_2O_7$ indicates that commensurate long-range magnetic order occurs below 150 K [16] and the magnetoresistance effect of $Nd_2Ir_2O_7$ shows that below T_c, because the conductivity is caused by an excitation from the all-in/all-out

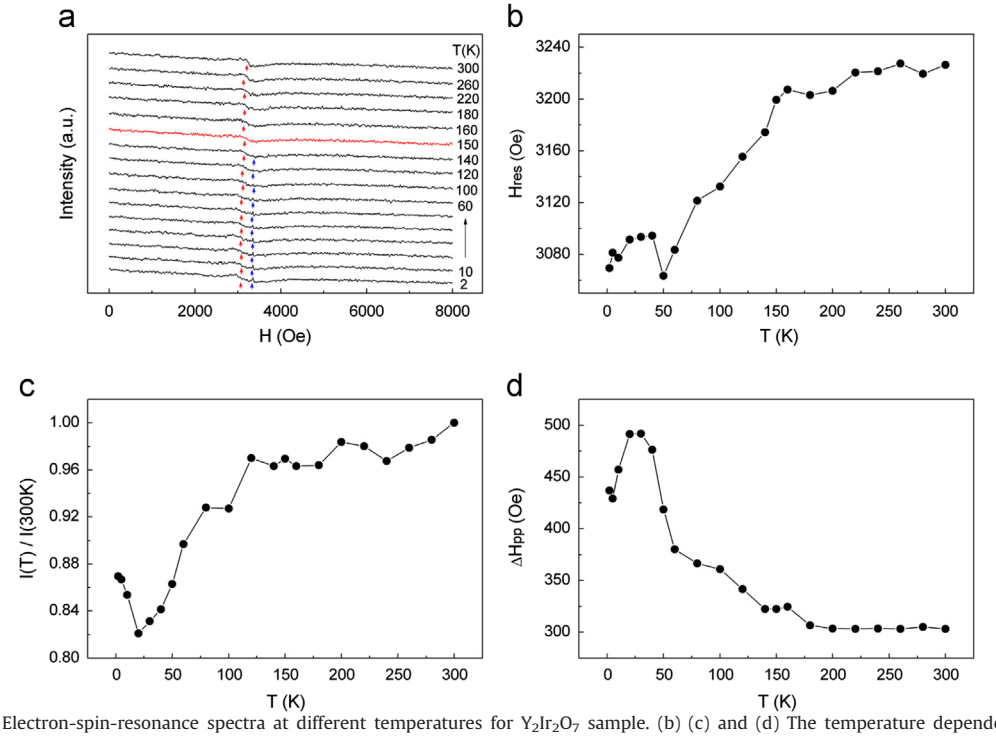

Fig. 3. (Color online) (a) Electron-spin-resonance spectra at different temperatures for $Y_2Ir_2O_7$ sample. (b) (c) and (d) The temperature dependence of the measured resonance field, relative intensity and the peak-to-peak width for the low-field peak (red arrow), respectively.

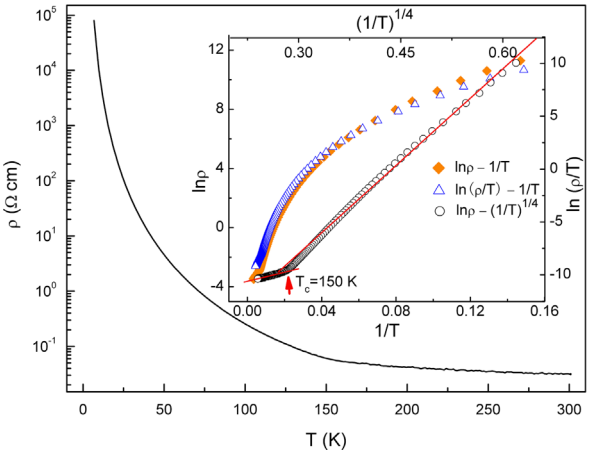

Fig. 4. (Color online) Resistivity of $Y_2Ir_2O_7$ as a function of temperature. The inset shows the fits to activated behavior model (orange diamond), small polarons model (blue triangle), and VRH model (black circle), respectively.

state, the mechanism of conductivity must be VRH [27]. Therefore, we believe that AFM fluctuation leads to the VRH process in the range of $T < T_c$. In the temperature range of $T > T_c$, the VRH also dominates the conductivity behavior possibly due to the thermal fluctuations and an intermediate glasslike or short-range ordered phase in $Y_2Ir_2O_7$ as observed in $Nd_2Ir_2O_7$. These suggest that the insulating behavior in $Y_2Ir_2O_7$ should not be due to a gapped phase. Thus, localization effect due to disorder or collective excitation may be important to determine the insulating phase in this system. This is in agreement with the result of electronic structure calculations that the intensity of the spectral functions at ε_F is significantly weak [5]. It should be noticed that there is a drastic change of slope of $\ln \rho$–$(1/T)^{1/4}$ curve at $T_c = 150$ K, which may be due to the transition to the AFM order. Therefore, the magnetic transition is closely related to the nature of electron transport. Actually, the functions of photoemission spectra show a $|\varepsilon - \varepsilon_F|^{1.5}$ dependence suggesting an important role of electron–magnon coupling. This is natural as a large radial extension of the 5d orbitals would favor collective excitation modes [12]. From the transport property and the weak magnetic moment of $Y_2Ir_2O_7$, one can obtain that the electron spins form an AFM ordered state with all-in/all-out magnetic structure instead of FM alignment in the ground state.

4. Conclusion

In summary, we have studied the magnetic order, spin dynamics and transport properties of the pyrochlore iridate $Y_2Ir_2O_7$. This iridate is a unique frustration system that exhibits coexistence of ferromagnetic and antiferromagnetic component. The AFM order is attributable to Ir–O–Ir AFM superexchange interaction, while the FM component is caused by canting of the moments from the AFM state. The ESR measurement confirms that antiferromagnetic fluctuation is responsible for the existence of ferromagnetic component. The variable-range hopping process dominates the transport mechanism. Magnetic and transport properties reveal that the electron spins form an AFM ordered state with all-in/all-out magnetic structure instead of FM alignment in the ground state.

Acknowledgments

This work was supported by the State Key Project of Fundamental Research of China (Grant nos. 2010CB923403 and 2011CBA00111), the Nature Science Foundation of China (Grant nos. 11174290, U1232142 and U1332140), and the Hundred Talents Program of the Chinese Academy of Sciences.

References

[1] C. Cosio-Castaneda, P. de la Mora, F. Morales, R. Escudero, G. Tavizon, J. Solid State Chem. 200 (2013) 49.

[2] T.F. Qi, O.B. Korneta, X. Wan, L.E. DeLong, P. Schlottmann, G. Cao, J. Phys.: Condens. Matter 24 (2012) 345601.
[3] B.-J. Yang, Y.B. Kim, Phys. Rev. B 82 (2010) 085111.
[4] X. Wan, A.M. Turner, A. Vishwanath, S.Y. Savrasov, Phys. Rev. B 83 (2011) 205101.
[5] K. Maiti, Solid State Commun. 149 (2009) 1351.
[6] J.P. Clancy, N. Chen, C.Y. Kim, W.F. Chen, K.W. Plumb, B.C. Jeon, T.W. Noh, Y.-J. Kim, Phys. Rev. B 86 (2012) 195131.
[7] E.K.-H. Lee, S. Bhattacharjee, Y.B. Kim, Phys. Rev. B 87 (2013) 214416.
[8] H. Fukazawa, Y. Maeno, J. Phys. Soc. Jpn. 71 (2002) 2578.
[9] N. Taira, M. Wakeshima, Y. Hinatsu, J. Phys.: Condens. Matter 13 (2001) 5527.
[10] N. Aito, M. Soda, Y. Kobayashi, M. Sato, J. Phys. Soc. Jpn. 72 (2003) 1226.
[11] D. Yanagishima, Y. Maeno, J. Phys. Soc. Jpn. 70 (2001) 2880.
[12] R.S. Singh, V.R.R. Medicherla, K. Maiti, E.V. Sampathkumaran, Phys. Rev. B 77 (2008) 201102.
[13] M.C. Shapiro, S.C. Riggs, M.B. Stone, C.R. de la Cruz, S. Chi, A.A. Podlesnyak, I.R. Fisher, Phys. Rev. B 85 (2012) 214434.
[14] S. Zhao, J.M. Mackie, D.E. MacLaughlin, O.O. Bernal, J.J. Ishikawa, Y. Ohta, S. Nakatsuji, Phys. Rev. B 83 (2011) 180402.
[15] S.M. Disseler, C. Dhital, T.C. Hogan, A. Amato, S.R. Giblin, C. de la Cruz, A. Daoud-Aladine, S.D. Wilson, M.J. Graf, Phys. Rev. B 85 (2012) 174441.
[16] S.M. Disseler, C. Dhital, A. Amato, S.R. Giblin, C. de la Cruz, S.D. Wilson, M.J. Graf, Phys. Rev. B 86 (2012) 014428.
[17] K. Matsuhira, M. Wakeshima, R. Nakanishi, T. Yamada, A. Nakamura, W. Kawano, S. Takagi, Y. Hinatsu, J. Phys. Soc. Jpn. 76 (2007) 043706.
[18] J.J. Ishikawa, E.C.T. O'Farrell, S. Nakatsuji, Phys. Rev. B 85 (2012) 245109.
[19] K. Matsuhira, M. Wakeshima, Y. Hinatsu, S. Takagi, J. Phys. Soc. Jpn. 80 (2011) 094701.
[20] K. Miyoshi, Y. Nishimura, K. Honda, K. Fujiwara, J. Takeuchi, J. Phys. Soc. Jpn. 69 (2000) 3517.
[21] J.G. Zhao, L.X. Yang, Y. Yu, F.Y. Li, R.C. Yu, C.Q. Jin, Solid State Commun. 150 (2010) 36.
[22] X. Wan, A. Vishwanath, S.Y. Savrasov, Phys. Rev. Lett. 108 (2012) 146601.
[23] L. Zhang, H. Lei, X. Zhu, W. Tong, C. Zhang, Y. Zhang, C. Petrovic, Philos. Mag. 93 (2013) 1132.
[24] D. Tan, C. Zhang, C. Xi, L. Ling, L. Zhang, W. Tong, Y. Yu, G. Feng, H. Yu, L. Pi, Z. Yang, S. Tan, Y. Zhang, Phys. Rev. B 84 (2011) 014502.
[25] Y. Yu, C. Zhang, W. Tong, L. Zhang, D. Tan, L. Pi, Z. Yang, M. Tian, S. Tan, Y. Zhang, New J. Phys. 14 (2012) 023032.
[26] S. Yoshii, M. Sato, J. Phys. Soc. Jpn. 68 (1999) 3034.
[27] K. Matsuhira, M. Tokunaga, M. Wakeshima, Y. Hinatsu, S. Takagi, J. Phys. Soc. Jpn. 82 (2013) 023706.